Modeling, Simulation and Testing of a Magnetically Enhanced RF Plasma Source for a High Power Electromagnetic Thruster

IEPC-2019-398

Presented at the 36th International Electric Propulsion Conference
University of Vienna • Vienna, Austria
September 15-20, 2019

Xiaodong Wen[1], Lijuan Liu[2], Xinfeng Sun[3], Chenchen Wu[4], Yanhui Jia[5]
Science and Technology on Vacuum Technology and Physics Laboratory, Lanzhou Institute of Physics, Lanzhou 730000, China

Abstract: High Power Electromagnetic Thrusters are being widely developed to meet a variety of space propulsion requirements for future robotic and manned space missions. Recently, A 5 kW electromagnetic thruster prototype with a radio-frequency plasma source and a rotating magnetic field acceleration section is being developed at Lanzhou Institute of Physics (LIP). The plasma source is magnetically enhanced and inductively coupled with an RF antenna driven at 13.56 MHz. This paper presents the modeling, simulation and testing of the RF Xenon plasma source. A two-dimensional axial-symmetric model is established and a parameter of modified electron mobility is applied to simulate the RF discharge of the plasma source. Furthermore, the characteristics of the plasma source with varying the RF power, applied magnetic flux density and gas flow rate is tested in a vacuum chamber. It is demonstrated experimentally and theoretically that, with the applied magnetic flux of 100 G and the RF power up to 500 W, the electron number density and electron temperature are nearly 8×10^{18} - 4×10^{19} m^{-3} and 2.2 eV plasma can be achieved, which is suitable for the next-stage RMF acceleration.

Nomenclature

$\boldsymbol{B}_z$	=	axial static magnetic flux density
$\boldsymbol{B}_\omega$	=	RMF magnetic flux density
$\boldsymbol{D}_e$	=	electron diffusion coefficient
$\boldsymbol{D}_\varepsilon$	=	electron energy diffusion coefficient
$\boldsymbol{E}$	=	electric field strength vector
$\boldsymbol{H}$	=	magnetic field strength vector
I_{sp}	=	specific impulse
L_A	=	effective length of RMF acceleration section
n_e	=	plasma density
n_ε	=	electron energy density
Q_{abs}	=	absorbed RF power by plasma
R	=	effective radius of RMF acceleration section
RMF	=	rotating magnetic field

[1] Engineer, Science and Technology on Vacuum Technology and Physics Laboratory, wenxd510@163.com.
[2] Engineer, Science and Technology on Vacuum Technology and Physics Laboratory, liulj3000@126.com.
[3] Engineer, Science and Technology on Vacuum Technology and Physics Laboratory, xinfenghappy@126.com.
[4] Engineer, Science and Technology on Vacuum Technology and Physics Laboratory, wucc510@163.com.
[5] Senior Engineer, Science and Technology on Vacuum Technology and Physics Laboratory, jiayh510@163.com.

r_p	=	plasma radius
S_e	=	source or sink term of electrons
S_ε	=	the energy loss or gain due to inelastic collisions
T	=	thrust of an electric thruster
ω_{RMF}	=	angular driven frequency of RMF
$\boldsymbol{\mu}_e$	=	electron mobility tensor
$\boldsymbol{\mu}_\varepsilon$	=	electron energy mobility tensor
μ_{dc}	=	DC electron mobility
Γ_e	=	electron flux
Γ_ε	=	electron energy flux

I. Introduction

THe requirements on the high performance in-space propulsion system of spacecraft is becoming increasingly higher due to the he rapid increasing of space missions like deep space exploration, Mars landing, asteroid exploration and large-scale orbit transfer. For instance, higher I_{sp} is beneficial not only to substantially decreasing the propellants of the propulsion system and the launching mass of the rocket, but also to increasing the quantities of the payloads. For manned deep space exploration, high thrust is also indispensable to reduce the mission time and hence guarantee the astronauts' living and safety. High I_{sp} and high thrust, therefore, require the electric thruster to operate with high input power.

To meet the above requirements, several high power electric propulsions such as MPDT[1], PIT[2], NHT[3], VASIMR[4] and ELF[5] have been studied and developed extensively in past decades. Among these thrusters, ELF show great potentials to operate up to MW power levels due to its essential high energy density, which is derived from the Rotamak[6, 7], a concept of magnetic confinement nuclear fusion. Besides, beneficial from its electrodeless design, lightweight and compaction, ELF has extremely long operation lifetime while operating in such high power. Meanwhile, based on the pulsed creation, confinement and acceleration of a high-density, magnetized Field Reversed Configuration (FRC) plasmoid by employing a Rotating Magnetic Field (RMF), ELF thrusters can perform steadily over a very wide range of high power while keeping relatively high efficiencies.

A 5kW downscaled thruster prototype call Electrodeless Plasmoid Thruster (EPT) consisting of an inductive preionization (PI) stage and a RMF acceleration stage has been designed, fabricated and tested at Lanzhou Institute of Physics (LIP) in past few years as shown in Figure 1. The PI system is a RF plasma source with an inner diameter of 40 mm which is magnetically enhanced and inductively coupled with an RF antenna driven at 13.56 MHz. In order to optimize the PI system, a two-dimensional axisymmetric MHD model based on COMSOL has been established and some numerical calculations have been carried out. Besides, a preliminary experiment has been performed to verify and correct the simulation results. In this paper, the numerical model and calculation results are respectively presented in Sec. II and Sec. III, which is followed by the ignition experiment of PI system in Sec. IV. Finally, a conclusion is presented in Sec. V.

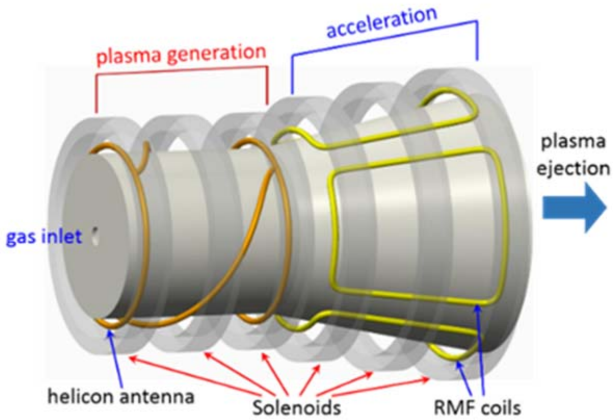

Figure 1. Schematic of the EPT.

II. Model description

The 2D axisymmetric simulation model established by COMSOL is shown in Figure 2. A 5-trun RF antenna driven at 13.56 MHz with a length of 30 mm is applied to couple with the plasma. The background axial magnetic field and gas pressure are both uniformly distributed with values of 100 Gauss and 2 Pa. The gas used in the simulation is Xenon.

A. Equations for Fluid Plasma Model

For the inductively RF plasma discharge, the momentum transfer collisional frequency is larger than the radio frequency (RF) driving frequency which is 13.56 MHz here. Thus the general flux balance equation for electrons can be instead by drift-diffusion (DD) approximation[8] which can be expressed as

$$\frac{\partial n_e}{\partial t} + \nabla \cdot \boldsymbol{\Gamma}_e = S_e \tag{1}$$

$$\frac{\partial n_\varepsilon}{\partial t} + \nabla \cdot \boldsymbol{\Gamma}_\varepsilon + \boldsymbol{E} \cdot \boldsymbol{\Gamma}_\varepsilon = S_\varepsilon + Q_{abs}/e \tag{2}$$

where S_e is the source terms for electrons and S_ε is he energy loss or gain due to inelastic collisions. $\boldsymbol{E} \cdot \boldsymbol{\Gamma}_\varepsilon$ is the change of the electron energy caused by the electric field $\boldsymbol{E}$. The electron flux $\boldsymbol{\Gamma}_e$ and electron energy flux $\boldsymbol{\Gamma}_\varepsilon$ are respectively defined as

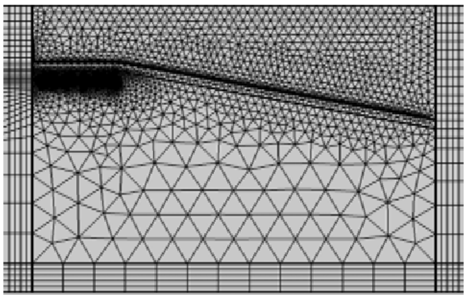

Figure 2. 2D simulation model of PI system.

$$\boldsymbol{\Gamma}_e = -n_e(\boldsymbol{\mu}_e \cdot \boldsymbol{E}) - \boldsymbol{D}_e \cdot \nabla n_e \tag{3}$$

$$\boldsymbol{\Gamma}_\varepsilon = -n_\varepsilon(\boldsymbol{\mu}_\varepsilon \cdot \boldsymbol{E}) - \boldsymbol{D}_\varepsilon \cdot \nabla n_\varepsilon \tag{4}$$

here $\boldsymbol{E}$ is the electric field strength which causes electrons movement with an electron mobility $\boldsymbol{\mu}_e$ and an electron energy mobility $\boldsymbol{\mu}_\varepsilon$, $\boldsymbol{D}_e$ and $\boldsymbol{D}_\varepsilon$ are electron diffusion coefficient and electron energy diffusion coefficient which causes electrons diffusion, in respectively. Assuming that the electrons have a Maxwellian distribution in the velocity phase space and the applied magnetic field only has a component in axil direction, the mobility here which is a tensor[9] satisfy

$$\mu_e = \frac{\mu_{dc}}{1 + B_z^2 \mu_{dc}^2} \begin{pmatrix} 1 & B_z\mu_{dc} & 0 \\ -B_z\mu_{dc} & 1 & 0 \\ 0 & 0 & 1 + B_z^2\mu_{dc}^2 \end{pmatrix} \tag{5}$$

where $\mu_{dc} = e/m_e(\nu_e + j\omega)$ is the scalar electron mobility[10] in the absence of the applied magnetic field and B_z is the axial component of the magnetic field vector, ν_e is electron collisional frequency both including electron-ion collision and electron-neutral collision which can be calculated using the equations expressed in Ref. 11.

As the skin depth of RF current driven at 13.56 MHz is only 18 μm in the copper antenna, the computation will be quite huge and slow with proper meshing. Fortunately, an impedance boundary condition can be introduced to dramatically reduce the computation. In this boundary condition, the electromagnetic field induced by a current source can be written as

$$\sqrt{\frac{\mu_0\mu_r}{\varepsilon_0\varepsilon_r - j\sigma/\omega}} \cdot \boldsymbol{n} \times \boldsymbol{H} + \boldsymbol{E} - (\boldsymbol{n} \cdot \boldsymbol{E})\boldsymbol{n} = 0 \tag{6}$$

where μ_r, ε_r and σ are respectively relative permeability, relative dielectric constant and conductivity of the helicon antenna, ω is the angular frequency of RF current.

Meanwhile, the electron flux boundary satisfy[12]

$$\Gamma_e = \frac{1}{4} n_e \bar{v}_e \tag{7}$$

$$\Gamma_\varepsilon = \frac{5}{3}\frac{n_\varepsilon \bar{v}_e}{4} \tag{8}$$

where $\bar{v}_e = \sqrt{8kT_e/\pi m_e}$ is average thermal velocity of electrons.

B. Plasma Chemical Reaction

During the RF PI plasma discharge processes for Xenon gas, there are 25 particle collision reactions and 4 surface reactions are under consideration as listed in Table 1, whose cross section data can be found in this literature[13].

No.	Formula	Reaction type	Δε (eV)
1	e+Xe→e+Xe	elastic collision	0
2	e+Xe→e+Xe1	excitation	8.315
3	e+Xe1→e+Xe	de-excitation	-8.315
4	e+Xe→e+Xe2	excitation	9.447
5	e+Xe2→e+Xe	de-excitation	-9.447

6	e+Xe→e+Xe3	excitation	9.58
7	e+Xe3→e+Xe	de-excitation	-9.58
8	e+Xe→2e+Xe+	ionization	12.13
9	e+Xe1→2e+Xe+	ionization	3.785
10	e+Xe2→2e+Xe+	ionization	2.653
11	e+Xe3→2e+Xe+	ionization	2.52
12	e+Xe1→e+Xe2	excitation	1.132
13	e+Xe2→e+Xe1	de-excitation	-1.132
14	e+Xe2→e+Xe3	excitation	0.133
15	e+Xe3→e+Xe2	de-excitation	-0.133
16	2e+Xe+→e+Xe3	excitation	-0.133
17	Xe3+Xe→Xe2+Xe	de-excitation	/
18	Xe2+Xe→Xe1+Xe	de-excitation	/
19	Xe1+Xe1→e+Xe+Xe+	ionization	/
20	Xe2+Xe2→e+Xe+Xe+	ionization	/
21	Xe1+Xe2→e+Xe+Xe+	ionization	/
22	Xe1→Xe	de-excitation	/
23	Xe2→Xe	de-excitation	/
24	Xe3→Xe	de-excitation	/
25	Xe3→Xe1	de-excitation	/
26	Xe1→Xe	surface de-excitation	/
27	Xe2→Xe	surface de-excitation	/
28	Xe3→Xe	surface de-excitation	/
29	e+Xe+→Xe	recombination	/

III. Simulation Results

The typical simulated electron density and energy distributions are shown in Figure 3 while the RF power ranges from 100 to 500 W and the axial magnetic field ranges from 0 to 300 Gauss. The profile along the radial direction of the electron energy and plasma potential is shown in Figure 4.

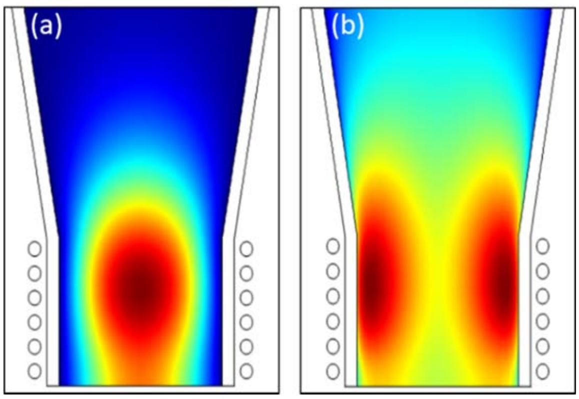

Figure 3. Electron density (a) and energy (b).

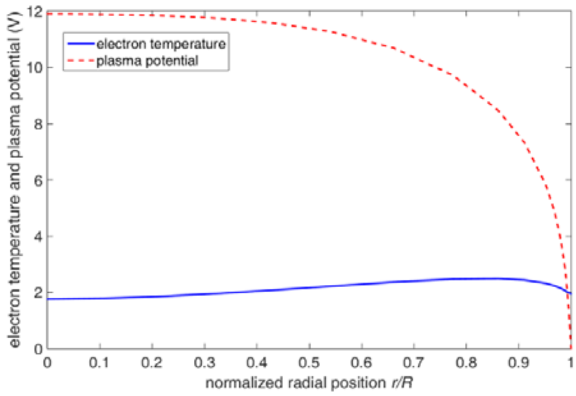

Figure 4. Profile of electron energy and plasma potential

According to the RF plasma theory, the plasma potential drop in the plasma pre-sheath and sheath can be respectively calculated by

$$V_{ps} = \frac{1}{2}\frac{T_e}{e} \tag{9}$$

$$V_s = \frac{1}{2}\frac{T_e}{e}\ln\left(\frac{M_i}{2\pi m_e}\right) \tag{10}$$

For Xenon, Eq. (10) is nearly to $5T_e/3e$. The average electron energies in the plasma pre-sheath and sheath are 1.9 eV and 2.3 eV as illustrated in Figure 4. Therefore, the total plasma potential drop is approximately equal to 13.14 V, which show great consistent with the simulation result 11.9 V as shown in Figure 4.

The effect of axial magnetic field to RF plasma discharge is shown in Figure 5 while the RF driven power is 300 W. On can see that higher density plasma can be obtained due to more efficient discharging when the applied magnetic field becoming much more intense. However, very high density is adverse to plasmoid acceleration in the RMF stage because the rotating magnetic field only penetrates in the very thin edge of the plasma column thus can not drive enough azimuthal plasma current to supply powerful Lorentz force. In this case, an applied magnetic field of nearly 100 Gs is enough for the next stage plasmoid acceleration.

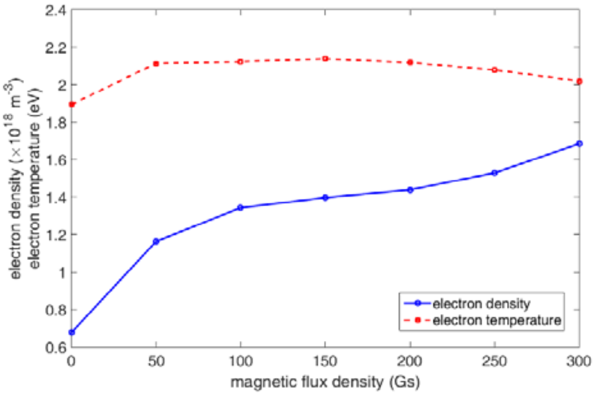

Figure 5. Variations of electron energy and density along with the magnetic field.

IV. Preliminary ignition experiment

The preliminary ignition experiment of PI system is carried out in the TS-6S vacuum chamber at LIP as shown in Figure 6(a). A single Langmuir probe located at the exit of the thruster is used to measure the plasma density and temperature of the plasma plume in the experiment as shown in Figure 6(b).


Figure 6. TS-6S vacuum chamber and Langmuir probe used in the experiment.

Figure 7(a) illustrate a typical image of the PI system plasma plume. The profiles of normalized plasma densities along z direction in the axis with different RF power are shown in Figure 7(b). The measured plasma densities at the exit of the thruster with different RF power are illustrated in Figure 8. The experimental results show great consistent with the simulation results which give some critical parameters of the PI system. Both experimental and simulation results also give a very important reference to develop the EPT thruster in the following work.

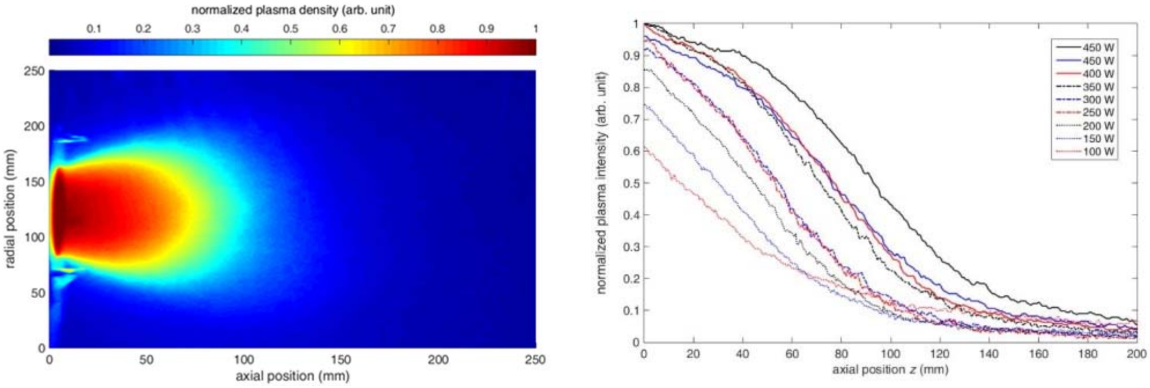

Figure 6. TS-6S vacuum chamber and Langmuir probe used in the experiment.

V. Conclusion

A 500 W RF PI source driven at 13.56 MHz has been designed and optimized by numerical solutions and verified by a preliminary experiment. The simulation results show that 8×10^{18} - 4×10^{19} m^{-3} and 2.2 eV plasma can be achieved, which is suitable for the next-stage RMF acceleration. Besides, the simulation results show great consistent with the experimental results and also give a very important reference to develop the EPT thruster in the following work. The PI plasma source will be further optimized to meet the requirements of RMF acceleration for the whole prototype thruster.

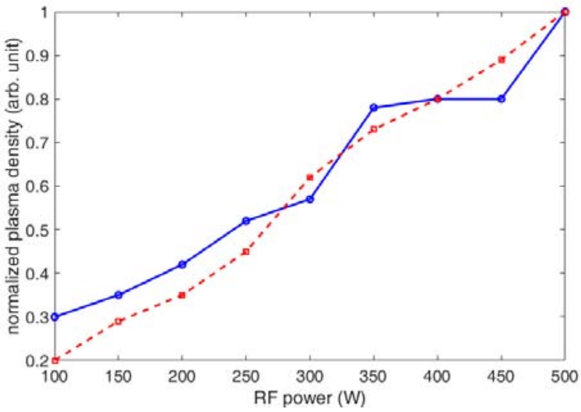

Figure 8. Normalized plasma densities with different RF power.

Acknowledgments

This work has been supported by National Natural Science Foundation of China (Grant No. 61701209, 11802111, and 61801201), Foundation of Innovative Research and Development of CASC (Grant No. 2018-686-15) and Foundation of Basic Research Project of SASTIND, China (Grant No. JCKY2018203B030).

References

[1] Yuya Oshio, Satoshi Tonooka, Ikkoh Funaki, "Thrust Performance and Cathode Temperature Evaluation of MW Class Quasi-Steady MPD Thruster," Proceedings of the 52nd AIAA/SAE/ASEE Joint Propulsion Conference, AIAA 2016-5039, Salt Lake City, 2016, pp. 1-11.

[2] Ashley K. Hallock, Adam K. Martin, Kurt A. Polzin, Adam C. Kimberlin, and Richard H. Eskridge, "Single- and Repetitive-Pulse Conical Theta-Pinch Inductive Pulsed Plasma Thruster Performance", IEEE Transactions on Plasma Science, Vol. 43, No. 1, 2015, pp. 433-443.

[3] S. J. Hall, B. A. Jorns, A. D. Gallimore, J. H. Gilland, P. Y. Peterson, and M. J. Baird, "High-power performance of a 100-kW class nested Hall thruster," Proceedings of the 35th International Electric Propulsion Conference, IEPC-2017-228, Atlanta, 2017, pp. 1-23.

[4] Jared P. Squire, Mark D. Carter, Franklin R. Chang Díaz, Lawrence Dean, Matthew Giambusso, Tim G. Glover, Jose Castro, and Juan Del Valle, "Advances in Duration Testing of the VASIMR® VX-200SS System", Proceedings of the 52nd AIAA/SAE/ASEE Joint Propulsion Conference, AIAA 2016-4950, Salt Lake City, 2016, pp. 1-10.

[5] Anthony P. Pancotti, Justin M. Little, Jordan S. Neuhoff, Barry M. Cornella, David E. Kirtley, and John T. Slough, "Electrodeless Lorentz Force (ELF) Thruster for ISRU and Sample Return Mission", Proceedings of the 34th International Electric Propulsion Conference, IEPC-2015-67, Hyogo-Kobe, Japan, 2015, pp. 1-10.

[6] Shuyan Xu, Mark Lim, Shiyong Huang, Luxiang Xu, Igor Levchenko and Kateryna Bazaka, "Highly Efficient Miniaturized Hall-Type Thruster and Rotamak Projects in Plasma Sources and Application Centre at the Nanyang Technological University, Singapore," Proceedings of the 35th International Electric Propulsion Conference, IEPC-2017-591, Atlanta, 2017, pp. 1-6.

[7] Daisuke Kuwahara, Shunjiro Shinohara, and Kazuki Yano, "Thrust characteristics of high-density helicon plasma using argon and xenon gases," Journal of Propulsion and Power, Vol. 33, No. 2, 2016, PP. 420-424.

[8] H. C. Kim, F. Iza, S. S. Yang, M. Radmilović-Radjenović, and J. K. Lee, "Particle and Fluid Simulations of Low-temperature Plasma Discharges: Benchmarks and Kinetic Effects," Journal of Physics D: Applied Physics, Vol. 38, No. 19, 2005, pp. R283-R301.

[9] Xiong Yang, Mousen Cheng, Dawei Guo, Moge Wang, and Xiaokang Li, "Characteristics of temporal evolution of particle density and electron temperature in helicon discharge," Plasma Sci. Technol., Vol. 19, 2017, pp. 105402.

[10] Chabert Pascal, Physics of Radio-Frequency Plasmas, Cambridge: Cambridge University Press, 2011, pp. 236.

[11] Hagelaar, G. J. M., and L. C. Pitchford, "Solving the Boltzmann equation to obtain electron transport coefficients and rate coefficients for fluid models," Plasma Sources Science and Technology, Vol. 14, No. 4, 2005, pp. 722.

[12] M. A. Lieberman, A. J. Lichtenberg, "Principles of Plasma Discharge and Materials Processing," New York: John Wiley, 2006, pp. 131.

[13] M. C. Bordage, S. F. Biagi, L. L. Alves, K. Bartschat, S. Chowdhury, L. C. Pitchford, GJM Hagelaar, W. L. Morgan, V. Puech and O. Zatsarinny, "Comparisons of sets of electron–neutral scattering cross sections and swarm parameters in noble gases: III. Krypton and xenon," J. Phys. D: Appl. Phys. Vol. 46, 2013, pp. 334003.